Geoderma 398 (2021) 115104

Contents lists available at ScienceDirect

Geoderma

journal homepage: www.elsevier.com/locate/geoderma

High-energy moisture characteristics of various low organic matter sandy soils in different land uses

Arezoo Sharifi [a,*], Hossein Shirani [a], Ali Asghar Besalatpour [b], Isa Esfandiarpour-Boroujeni [a], Mohammad Ali Hajabbasi [c]

[a] Department of Soil Science, Faculty of Agriculture, Vali-e-Asr University of Rafsanjan, Rafsanjan, Iran
[b] inter 3 Institute for Resource Management, Berlin, Germany
[c] Department of Soil Science, Faculty of Agriculture, Isfahan University of Technology, Isfahan, Iran

ARTICLE INFO

Handling Editor: Morgan Cristine L.S.

Keywords:
HEMC indices
Van Genuchten equation
Fractal dimension
Structural stability ratio
Soil water retention

ABSTRACT

Soil structure serves as one of the most important soil physical properties influencing on water retention, aeration, plant growth as well as environmental conditions. In the current study, the effect of four land-use types on some soil structural stability indices including high-energy moisture characteristic (HEMC) at both fast and slow wetting modes, volume of the drainable pores (VDP), structural index (SI), stability ratio (SR), fractal dimensions (D) and mean weight diameter (MWD) was investigated. Jiroft County, is located in southeastern part of Kerman Province, Iran (28° 40′ N, 57° 44′ E) and characterized by soils generally high in sand and low in organic matter (OM) was selected as the study area. Land-use types included disturbed and undisturbed rangelands, protected natural forest and an artificial forest plantation. The HEMC results showed that in the slow wetting mode, undisturbed rangeland (49.6%) and protected natural forest (42.6%) indicated the highest and lowest values for near-saturated water contents, respectively. However, in fast wetting modes no significant differences was observed in case of near-saturated water content between undisturbed rangeland and disturbed rangeland and artificial forest plantation land-uses. Furthermore, the near-saturated water contents in the protected natural forest did not changed for both fast and slow wetting modes. The lowest MWD (0.05 mm) and the highest fractal dimension values (2.97) were observed for protected natural forest. The lowest values for VDP, VDP ratio (VDPR), and SI were found for undisturbed rangeland and disturbed rangeland, with the highest values obtained for protected natural forest. No significant differences were found among the land-use types in terms of SR. Furthermore, soil water retention was also low in the land use types with low aggregate formation agents like clay, OM, and calcium carbonate equivalent (CCE). Among the HEMC indices, near-saturated water content and soil water retention only indicated the structural condition. While other HEMC indices such as VDP, SI, S_iR, and VDPR did not show the differences between structural and textural characteristics. This study revealed that, techniques such as measuring MWD and fractal dimension may better show the status of the soil aggregates in the studied region.

1. Introduction

As a key feature of soil physical quality (Dlapa et al., 2011; Castro Filho et al., 2002), soil structure comes from the coalescence of primary particles and the formation of secondary constituents called aggregates (Kelishadi et al., 2018). Soil structure is usually expressed through aggregate stability which significantly affects soil fertility, plant nutrition and root environment in general. Aggregate stability means the ability of soil structure to resist against destructive forces operating on it such as water (Hillel, 1982). Aggregate stability varies by several factors such as organic matter (Brtnicky et al., 2017), soil tillage, decomposition rate of organic matter, microbial activities, plant roots (Hosseini et al., 2015), soil management practices and vegetation type (Avanzi et al., 2011), soil texture, porosity, temperature, as well as land-use patterns (Zhang et al., 2008). In turn, soil structure and aggregate stability can influence soil biological and physical properties such as soil porosity, permeability, and aeration (Le Bissonnais, 1996; Zheng et al., 2011a,

* Corresponding author.
E-mail addresses: Arezoo.sharifi@stu.vru.ac.ir (A. Sharifi), Shirani@vru.ac.ir (H. Shirani), a_besalatpour@yahoo.com (A.A. Besalatpour), esfandiarpoor@vru.ac.ir (I. Esfandiarpour-Boroujeni), hajabbas@cc.iut.ac.ir (M.A. Hajabbasi).

https://doi.org/10.1016/j.geoderma.2021.115104
Received 5 January 2020; Received in revised form 10 March 2021; Accepted 21 March 2021
Available online 6 April 2021

Nomenclature

Abbreviation	Description	Unit
OM	Organic matter	Kg 100Kg^{-1}
BD	Bulk density	g cm^{-3}
CCE	Calcium carbonate equivalent	Kg 100Kg^{-1}
D	Fractal dimension	
MWD	Mean weight diameter	mm
HEMC	High energy moisture characteristic	
SI	Structural index	hPa^{-1}
SR	Stability ratio	
VDP	Volume of drainable pores	g g^{-1}
VDPR	Ratio of fast wetting to slow wetting VDP values	
C(θ)	Specific water capacity function	hPa^{-1}
θ	Gravimetric water content	g g^{-1}
θ_s	Predicted *pseudo* saturated water content	g g^{-1}
θ_r	Predicted *pseudo* residual water content	g g^{-1}
h	Matric suction	hPa
S_i	Slope at the infection point of HEMC	hPa^{-1}
S_iR	Ratio of fast wetting to slow wetting S_i values	

2011b; Gholoubi et al., 2019).

Various approaches have been proposed for measuring aggregate stability (Le Bissonnais, 1996), for example, indices such as aggregate fractal dimension (Zheng et al., 2011a, 2011b; Ding and Huang, 2017), mean weight diameter (MWD), geometric mean diameter (GMD), water-stable aggregation (WSA), dispersible clay (DC), aggregate stability index (ASI) (Saygın et al., 2012), and ultrasonic energy (Levy and Mamedov, 2002). Because of some restrictions faced by previous methods for determining aggregate stability, a more recent technique, high-energy moisture characteristic (HEMC), was proposed by Childs (1940) and further modified by Collis-George and Figuera (1984), Pierson and Mulla (1989), and Levy and Mamedov (2002). The HEMC method, which means the water release curve at high energies (i.e. low matric suctions), is a highly sensitive and efficient method for detecting even small differences in aggregate stability (Crescimanno et al., 1995; Avanzi et al., 2011). Management practices may alter soil structure and aggregate properties, and as a consequence would change the shapes of HEMC. Recently, HEMC has been considered as one of the most practical and suitable methods for determining structural stability of soils in arid and semi-arid regions with a wide range of stability levels. In fact, HEMC is mostly applicable for soils with weak structural stability, for example sandy soils, in which structural stability is also highly difficult to be described by conventional methods (Baiamonte et al., 2019). HEMC is sensitive to the pore size distribution, and how easily gravitational water moves through the soil. Not only the HEMC is depended on the soil structure but it also could be influenced by texture (Hosseini et al., 2015) so that even small changes in the soil stability (Avanzi et al., 2011) and soil textural components (Levy and Miller, 1997) can result in changes on the curve's shape.

Some studies have shown that forest and grassland land-use types could lead to increased stability of water-stable aggregates (Tang et al., 2016), while other studies have reported no significance effect of forest plantation on soil structural stability indices compared to native vegetation (Avanzi et al., 2011). Delelegn et al (2017) investigated the effects of five land-use types including natural forest, cropland, grassland, exclosure area, and eucalyptus plantation on soil quality indices and showed that conversion of natural forest to cropland and grassland resulted in decline in soil quality and aggregate stability. However, compared to the cropland, establishment of exclosure area and agro-forestry on degraded land could restore soil quality and aggregate stability. In case of Iran, Baranian Kabir et al. (2017) reported better conditions for aggregate stability indices in the central rangelands of Iran compared to arid and abandoned lands.

Not only soil structure but also soil textural components could influence on HEMC and its indices. More specifically, the sandy soils seem to represent similar behavior as the well-structured soils in terms of HEMC. Few researches have been carried out on aggregate stability and its indices in case of sandy soils under natural resources in Iran. Therefore, this research aimed to measure and evaluate the variability in the aggregate stability indices such as HEMC in four different land use types of Jiroft County characterized by high percentage of sand and low organic matter content.

2. Materials and methods

2.1. Study area

Jiroft County occurred in southeastern part of Kerman province, Iran, (28° 40′ N and 57°44′ E). The region is of great importance not only in terms of agricultural activities, but also in case of natural resources (forest and rangeland). For example, the region is dominated by *Tecomella undulata* (Anar Sheitan) forest, a rare and valuable tree species. The region is characterized by very warm temperatures in summer and mild temperatures in winter with mean elevation of 650 m above sea level. Four different land-uses defined for the current study included: disturbed Farrash rangeland, undisturbed Marghzar rangeland, Anar-Sheitan protected forest and Tal-Siah artificial forest plantation (Fig. 1).

With an area of 10935 ha, Farrash rangeland (L1) is located at 80 km apart from northwest of Jiroft city with mean annual precipitation and temperature of 392.5 mm and 15.4 °C, respectively. The rangeland is dominated by the two major vegetation types of *Artemisia-Astragalus* and *Artemisia*. Other species in this region includes *Salsola*, *Calligonum*, *Peganum harmala*, *Alhagi*, *Hordeum murinum*, *Rheum*, *Cuminum cyminum*, *Pistacia atlantica*, *Prunus scoparia*, etc. (Sabznegar Afaq Co., 1999).

Marghzar rangeland (L2) is located at 85 km apart from north of Jiroft city, with an area of 5802 ha characterized dry climate and mean annual precipitation and mean annual temperature of 346.44 mm 19.5 °C, respectively. The vegetation types in foothills and hills are dominated by *Artemisia*, *Astragalus*, and *Stipa* (*Zannichellia palustris* and *Stipa barbata*) species, while, the dominant species in highland areas are *Artemisia* and *Astragalus*. A typical piedmont plain and floodplain area is dominated by species such as *uphorbia*, *Erythronium caucasicum*, and *Peganum harmala*. Species like *Allium schoenoprasum*, *Achillea millefolium*, *Bromus*, *Carex*, *Zannichellia palustris*, *Teucrium*, *Rosa canina*, *Ziziphora*, are also found in this region (Saman Sabz Ariyan Consulting Engineers, 2008).

With an area of 40 ha and dominated by *Tecomella undulata* species, Anar Sheitan (L3) is a protected forest located at 25 km apart from north of Jiroft city which serves as the largest forest reserve and one of the most famous habitats in the region. . *Tecomella undulata* is a rare species of the *Bignoniaceae* family. The climate is warm and semi-temperate, with a mean annual rainfall of 180 mm which almost occurs in winter. The region is characterized by very hot summers and mild winters, with minimum temperature rarely drops below 0 °C. The soil under these tree species is relatively deep, with sandy to sandy loam texture and often gravelly (Amiri et al., 2019).

Tal Siah area (L4) is located at 5 km from southwest of Jiroft city, with an area of 2539 ha. According to Jiroft weather station statistics mean annual rainfall, and maximum and minimum temperatures in this site are 173.5 mm, 49 and −4°C, respectively. The plant species in this area include *Ziziphus*, *Prosopis*, *Cabulica*, *Calligonum*, and *Cuminum cyminum*. The area has a dominant species of *Ziziphus* species with presence of other species at lower densities all over the region (Roodab Paydar Consulting Engineers, 2011).

2.2. Sampling and sample preparation

Topographic (1: 25000) and land-use maps were utilized for the

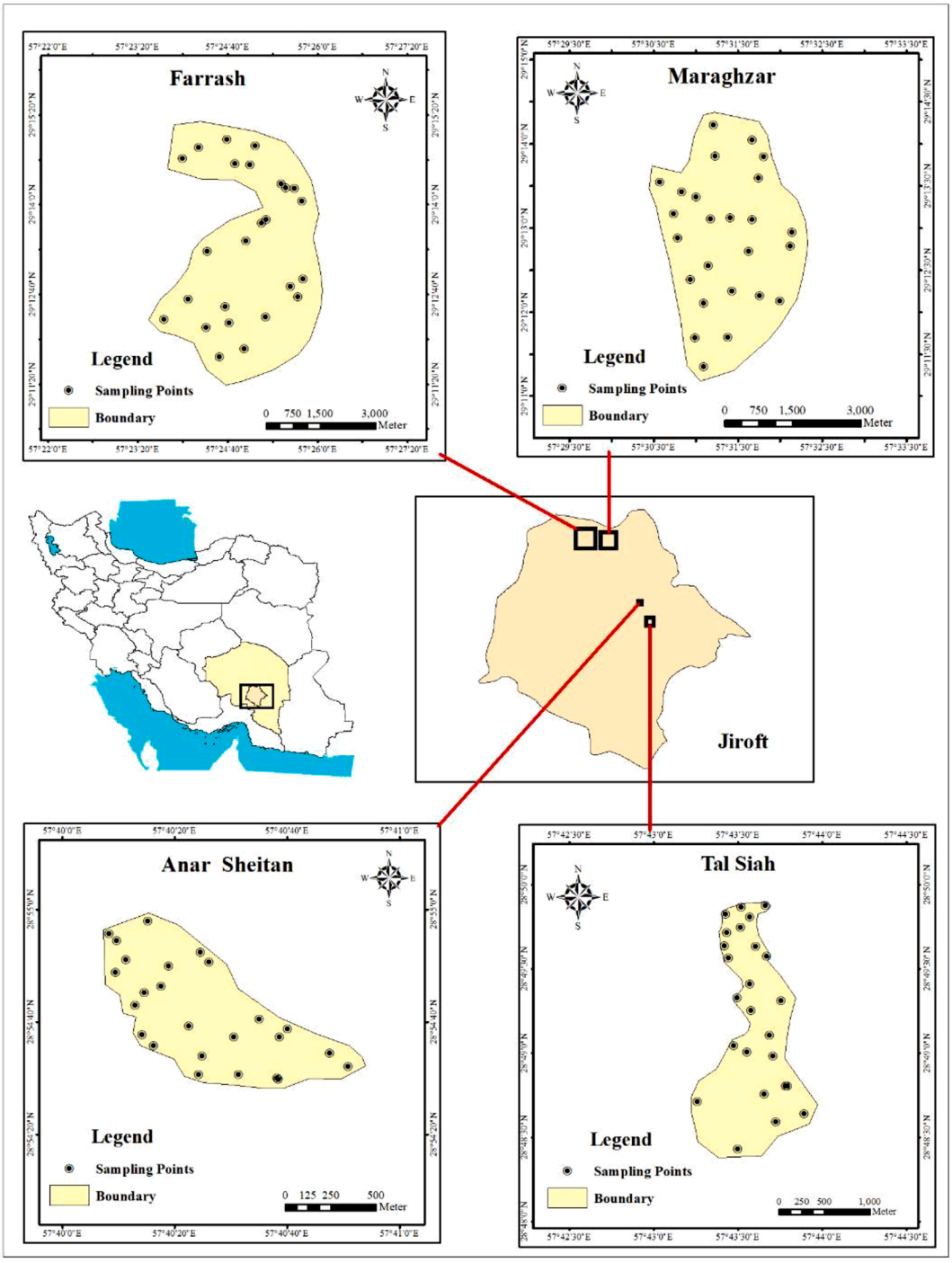

Fig. 1. The sampling points for the land use locations of Farrash (disturbed rangeland), Marghzar (undisturbed rangeland), Anar Sheitan (protected forest) and Tal Siah (artificial forest planttion).

initial identification of sampling points. A number of 25 sampling points was specified for each land-use type including natural forest, artificial forest plantation, disturbed rangeland and undisturbed rangeland (totally 100 sampling points). Soil samples (both disturbed and undisturbed samples) were taken from the surface horizon (0–10 cm) to study soil physical and chemical properties. Disturbed samples were collected with Auger, and the undisturbed with cylinders 5 cm in diameter and the height. The disturbed samples were air-dried and left for physical and chemical analysis.

2.3. Characterization of soil physical and chemical properties

Soil samples were sieved with a 4-mm sieve for the soil structural analysis, and a 2-mm sieve for characterizing other soil properties. Soil EC (Rhoades, 1996) and pH were measured in saturated extracts (McLean, 1982). Soil calcium carbonate equivalent (CCE) was obtained by back-titration with NaOH (Sims, 1996). Soil texture was determined by the hydrometer method (Gee and Bauder, 1986) and organic carbon by wet oxidation method (Nelson and Sommers, 1996) and bulk density (BD) using cylindrical method (Blake and Hartage, 1986).

2.4. High-energy moisture characteristic and HEMC data modeling

To determine aggregate stability by high-energy moisture characteristic technique, five grams of air-dried aggregates (0.5 to 1 mm in size) were placed in PVC cylinders (Mamedov, 2014; Hosseini et al., 2015; Saffari et al., 2020) and wetted in two series either slowly or quickly. After that, the water characteristic curves of the two series were determined by 2–3 hPa increment at different matric suctions (h) in the range of 0 to 50 hPa using a sandbox apparatus (Eijkelkamp, The Netherlands). The samples were weighed at each h and after equilibrium. Finally, the samples were dried at 105 °C in the oven, and gravitational water content (θ, g g^{-1}) at each matric suction was determined (Mamedov, 2014; Hosseini et al., 2015; Kelishadi et al., 2018). According to the previous studies (Hosseini et al., 2015) which have shown a significant correlation between the model parameters and structural indices of the two modified van Genuchten and van Genuchten models (Pierson and Mulla, 1989), these models were fitted to measured high-energy moisture characteristic (θ vs. h) data. The modified van Genuchten model (Eq. 1) was fitted to the HEMC data using the Excel Solver tool:

$$\theta(h) = \theta_r + (\theta_s - \theta_r)[1+(\alpha h)^n]\left(\frac{1}{n}-1\right) + Ah^2 + Bh + C \quad (1)$$

where, θ_s and θ_r are the *pseudo* saturated and residual water contents (g g^{-1}), h is matric suction (hPa), α (hPa^{-1}) and n (dimensionless) are the fitting parameters which control position and steepness of water retention curve, respectively, and A (hPa^{-2}), B (hPa^{-1}), and C (g g^{-1}) are the quadratic coefficients for improve model fitting to the measured data, respectively. After modeling the high-energy moisture characteristic, the soil structural index (SI, hPa^{-1}) in both fast and slow wetting modes were calculated by Eq. (2) (Mamedov et al., 2017).

$$\mathrm{SI} = \frac{\mathrm{VDP}}{h_{\mathrm{modal}}} \quad (2)$$

where, VDP is the volume of the drainable pores (g g^{-1}), and modal suction (h_{modal}, hPa) is the matric suction (h) at the peak of the specific water capacity content (C(θ)). The specific water capacity content [C(θ) = $|d\theta/dh|$, hPa^{-1}] was computed as the first derivative of Eq. (1) using Eq. (3):

$$\mathrm{C}(\theta) = \left|\frac{d\theta}{dh}\right| = (\theta_s - \theta_r)[1 + (\alpha h)^n]^{\left(\frac{1}{n}-1\right)}\left(\frac{1}{n}-1\right)(\alpha h)^n n\left(\frac{n}{h[1+(\alpha h)^n]}\right) + 2Ah + B \quad (3)$$

The VDP value is the bounded area between the pore shrinkage line (2Ah + B) and The specific water capacity curve C(θ), which was calculated by integrating through Simpson's method using Eq. (4):

$$VDP = \frac{\Delta x}{3}(y_0 + 4(y_1 + y_3 + y_5 + \ldots.) + 2(y_2 + y_4 + y_6 + \ldots.) + y_k) \quad (4)$$

where, Δx is the difference between two consecutive matric suctions, k is the number of subintervals in the desired matric suction domain whose value must be an even number, and y is the difference between the C(h) and the shrinkage line per matric suction. To calculate the modal suction (h_{modal}, hpa), the second derivative of Eq. (1) is set to zero (Eq. 5):

$$\frac{d^2\theta}{dh^2} = (\theta_S - \theta_r)\left(\frac{1}{\mathrm{n}}-1\right)\left(\frac{1}{\mathrm{n}}-2\right)n^2\alpha^2(\alpha h)(2n-2)[1+(\alpha h)^n]^{\left(\frac{1}{n}-3\right)} + (\theta_S - \theta_r)\left(\frac{1}{n}-1\right)(n-1)n\alpha 2(\alpha h)(\mathrm{n}-2)[1+(\alpha h)^n]^{\left(\frac{1}{n}-2\right)} + 2\mathrm{A} = 0 \quad (5)$$

since the value of A is very small, its effect on the h_{modal} value can be neglected, and the h_{modal} value can be calculated according to Eq. (6):

$$h_{modal} \approx \frac{1}{\alpha}\left(\frac{n-1}{n}\right)1/n \quad (6)$$

By calculating the structural index in both fast wetting (SI_{FW}) and slow wetting (SI_{SW}) modes, the stability ratio (SR) is calculated using Eq. (7) (Collis-George and Figueroa, 1984; Pierson and Mulla, 1989; Levy and Mamedov, 2002):

$$\mathrm{SR} = \frac{\mathrm{SI_{FW}}}{\mathrm{SI_{SW}}} \quad (7)$$

Furthermore, VDPR which is the ratio of VDP values in both fast wetting (VDP_{FW}) and slow wetting (VDP_{SW}) modes was used as another index to evaluate aggregate stability in this study:

$$\mathrm{VDPR} = \frac{\mathrm{VDP_{FW}}}{\mathrm{VDP_{SW}}} \quad (8)$$

S_i (hPa^{-1}), a structural stability index which is equal to the absolute value of the slope at the inflection point of HEMC (Hosseini et al., 2015; Saffari et al., 2020) was obtained by Eq. (9). By calculating the S_i ratio in both fast wetting ($S_{i\text{-}FW}$) and slow wetting ($S_{i\text{-}SW}$) modes, the S_iR index was applied to determine aggregate stability, Eq (10):

$$S_i = \left|\frac{d\theta}{dh}\right| = (\theta_s - \theta_r)\times \mathrm{n}\alpha \times \left(\frac{n-1}{2n-1}\right)^{\left(\frac{2n-1}{n}\right)} \quad (9)$$

$$\mathrm{SiR} = \frac{\mathrm{S_{i-FW}}}{\mathrm{S_{i-SW}}} \quad (10)$$

2.5. MWD indices of aggregates and fractal dimension

To measure the MWD indices of the aggregates by wet sieve method, 50 g of the soil passed through a 4-mm sieve, then gently transferred to the top-most sieve of the set 2, 1, 0.5, 0.25, and 0.1 mm (ASTM standard) and sieving was performed. Vertical sieving oscillation was 37 mm at 30 rpm for 3 min (van Bavel, 1950). The fractions remaining on the sieves were oven-dried at 105 °C for 24 h, weighed, and corrected for the sand fraction equal to/or greater than the corresponding sieve pore size to obtain the true proportion of the soil aggregates. Mean size of the aggregates retained by each sieve was computed according to the diameters of the adjacent sieves and MWD of the soil samples was calculated according to the van Bavel equation (1950) using Equation (10):

$$MWD = \sum_{i=1}^{n} w_i \bar{x}_i \quad (10)$$

where $\bar{x}_i$ is the mean diameter of the aggregates remaining on the sieve, w_i is the ratio of the aggregate weight remaining on each sieve to the total weight, and n is the number of sieves.

Soil samples were prepared to determine the fractal dimension of water-stable aggregates. Fractal dimension was calculated using the model reported by Yang et al (1993) (Eq. 10):

$$\frac{M(r < R_i)}{M_T} = \left(\frac{R_i}{R_{max}}\right)^{3-D_m} \quad (11)$$

where, M ($r < R_i$) is the cumulative mass of the smallest aggregates to the i class, M_T is the total mass, R_i is the mean aggregate diameter (in mm) in class i, R_{max} is the mean diameter of the largest aggregate, and D_m is the fractal dimension of aggregates. By deriving the logarithm of both sides of the above equation, the following linear equation is obtained:

$$Log\frac{M(r<R_i)}{M_T} = (3 - D_m)log\left(\frac{R_i}{R_{max}}\right) \quad (12)$$

Then, the fractal dimension was extracted from the slope of this line.

2.6. Statistical analysis

The SPSS 25 software was used for statistical analysis and comparison of mean values of different parameters for the land-use types was carried out using least significant different (LSD) test. Pearson correlation was used for investigating the relation between the variables as the data was normally distributed (Table 4). The diagrams from data were drawn by Microsoft Excel 2016 software.

3. Results and discussion

The HEMC indices and other soil structural properties were differently affected by the four land-use types. These changes will be discussed in detail as follows.

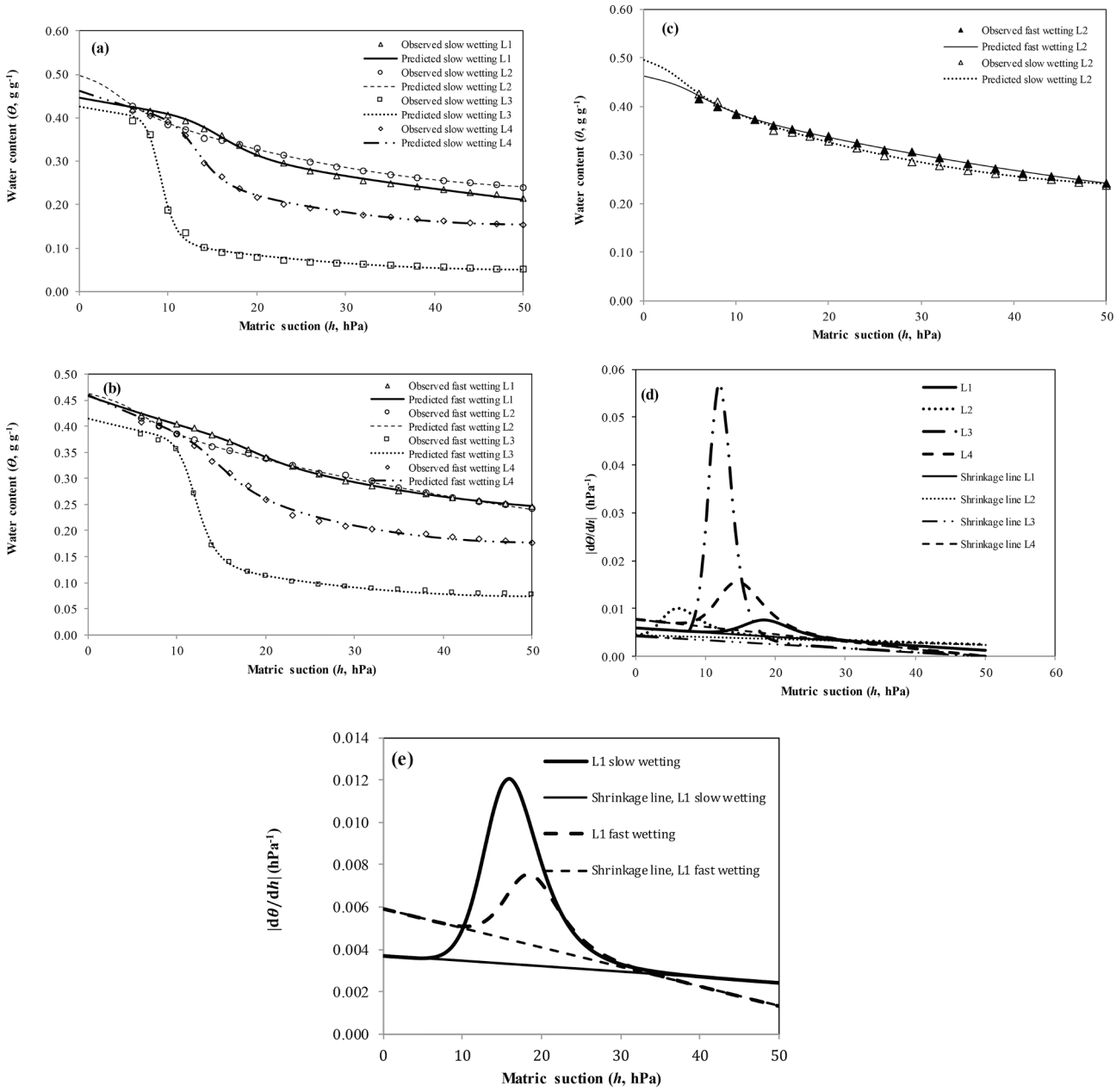

Fig. 2. Examples (For L1 land-use the sample no. 25 was selected, for L2 the sample no. 5, for L3 the sample no. 5, and for L4 the sample no. 9.) of high energy moisture characteristics (HEMC) (a) in slow wetting mode with predicted and observed data, (b) in fast wetting mode with predicted and observed data, (c) a comparison of both fast and slow wetting mode in undisturbed rangeland, (d) soil specific water capacity in different land uses, and (e) a comparison of soil specific water capacity in both fast and slow disturbed rangeland modes.

Table 1
The mean comparison of some soil properties of the studied land-uses.

Gravel	Sand	Clay	OM	BD (g cm^{-3})	EC (dS m^{-1})	pH	Soil texture	Location	Land-uses
(Kg $100Kg^{-1}$)									
29.6^{c}	59.12^{c}	14.4^{b}	0.2^{b}	1.52^{b}	3.9^{b}	8.21^{a}	Sandy loam	Disturbed rangeland, Farrash	L1
28.7^{c}	48.6^{d}	17.36^{a}	0.57^{a}	1.43^{c}	3.5^{b}	8.1^{b}	Loam, Sandy loam	Undisturbed rangeland, Marghzar	L2
42.9^{a}	77.28^{a}	9.28^{c}	0.25^{b}	1.58^{a}	4.8^{a}	8.18^{ab}	Sand, Loamy sand, Sandy loam	Protected forest, Anar Sheitan	L3
35.8^{b}	62.4^{b}	14.48^{b}	0.22^{b}	1.52^{b}	4.7^{a}	8.24^{a}	Sandy loam	Artificial forest plantation, Tal siah	L4

Similar letters indicate that there is no significant difference between land-use types. BD and OM are bulk density and organic matter, respectively.

Table 2
Statistical description of MVG model fitting parameters.

	Fitting parameters	Min	Max	Mean	SD	CV (%)
Slow	θ_r (g g^{-1})	0.033	0.336	0.188	0.075	39
	θ_s (g g^{-1})	0.189	0.426	0.324	0.048	14.8
	α (hPa^{-1})	0.053	0.473	0.154	0.089	57.8
	n (–)	2.8	15.0	6.37	3.25	51
	A (hPa^{-2})	−0.00002	0.00012	0.000055	0.000024	44
	B (hPa^{-2})	−0.011	−0.00016	−0.0058	0.0022	–
	C (g g^{-1})	0.036	0.287	0.155	0.055	35
	$\theta_{s\text{-Observed}}$ (g g^{-1})	0.366	0.666	0.474	0.061	12.8
Fast	θ_r (g g^{-1})	0.039	0.318	0.191	0.075	39
	θ_s (g g^{-1})	0.154	0.384	0.299	0.044	14.7
	α (hPa^{-1})	0.041	0.305	0.128	0.069	54
	n (–)	1.52	16.5	7.29	3.48	47.7
	A (hPa^{-2})	00,000	0.00011	0.000053	0.000023	43
	B (hPa^{-2})	−0.0111	−0.0018	−0.0057	0.0021	–
	C (g g^{-1})	0.059	0.28	0.156	0.052	33
	$\theta_{s\text{-Observed}}$ (g g^{-1})	0.285	0.592	0.454	0.0556	12.3

θ_r and θ_s are pseudo residual and saturated water contents, respectively, α and *n* are the fitting parameters which control position and steepness of HEMC, respectively, A, B and C are quadratic fitting coefficients. $\theta_{s\text{-Observed}}$ is water content measured at *h* value of 2 hPa.

3.1. HEMC indices in different land-use types and their relationships with soil properties

Examples of HEMC and specific water capacity curves in fast and slow wetting mode in different land uses are shown in Fig. 2a, b, c, d and e. These examples were chosen as they had a better fitting compared to the other land-use sampling points. Results illustrated good fitting of the modified van Genuchten model (Eq. (1)) to the measured HEMC data ($R^2 > 0.99$) (see Fig. 2).

Table 2 shows the statistical description of HEMC parameters in fast and slow wetting modes for both modified and original van Genuchten models. This Table indicates that in both fast and slow wetting conditions, the lowest and the highest coefficient of variations were found for θ_s and α, respectively. Additionally, the values of the fitting parameters for both modified and original van Genuchten models in the fast and slow wetting modes are given in Table 3.

The comparisons of slow wetting water retention curves for the four studied land-use types indicated a higher near-saturated water content ($\theta_{s\text{-Observed}}$), more α and θ_r and less *n* values for the undisturbed rangeland (L2) compared to other land-use types (Fig. 2a, Table 3). Mamedov (2014) stated that the soil sensitivity to disintegration decreased with increasing clay content and solution salinity, so that clayey soils are characterized by higher θ_s and α and lower *n* values compared to loamy soils as well as soils with more stable aggregates. Compared to other land-use types, the undisturbed rangeland represented a higher number and larger aggregates (larger MWD and smaller fractal dimension) due

Table 3
Fitting parameters of the modified van Genuchten (MVG) model and original van Genuchten (VG) model for soil examples in different land uses.

	Fitting parameters	L1,Soil no. 25		L2, Soil no. 5		L3, Soil no. 5		L4, Soil no. 9	
		MVG model	VG model	MVG model	VG model	MVG model	VG model	MVG model	VG model
Slow	θ_r (g g^{-1})	0.2114	0.0001	0.2405	0.0001	0.05037	0.06490	0.1538	0.1539
	θ_s (g g^{-1})	0.2945	0.4536	0.2938	0.5001	0.3350	0.4192	0.2866	0.4410
	α (hPa^{-1})	0.0614	0.0566	0.2036	0.1346	0.1089	0.1062	0.0748	0.0771
	n (–)	7.1871	1.5493	3.4252	1.3767	11.5394	7.7874	9.5856	4.0468
	A (hPa^{-2})	0.000013	–	0.000062	–	0.000037	–	0.000070	–
	B (hPa^{-2})	−0.00369	–	−0.00716	–	−0.00367	–	−0.0070	–
	C (g g^{-1})	0.1528	–	0.2025	–	0.09169	–	0.1752	–
	$\theta_{s\text{-Observed}}$ (g g^{-1})	0.4579	0.4529	0.4819	0.4819	0.4299	0.4299	0.4602	0.4603
Fast	θ_r (g g^{-1})	0.2468	0.0004	0.2409	0.0010	0.07442	0.0846	0.1768	0.1592
	θ_s (g g^{-1})	0.2769	0.4601	0.2868	0.4651	0.3089	0.4025	0.2651	0.4382
	α (hPa^{-1})	0.0529	0.0624	0.150000	0.0896	0.0824	0.0828	0.0664	0.0729
	n (–)	8.7167	1.6502	3.7430	1.397	11.4601	6.7344	7.2626	3.1506
	A (hPa^{-2})	0.000046	–	0.000021	–	0.000043	–	0.000078	–
	B (hPa^{-2})	−0.00594	–	−0.00457	–	−0.00427	–	−0.0078	–
	C (g g^{-1})	0.1816	–	0.1756	–	0.1068	–	0.1950	–
	$\theta_{s\text{-Observed}}$ (g g^{-1})	0.4529	0.4579	0.4649	0.4649	0.4255	0.4256	0.4559	0.4409

θ_r and θ_s are pseudo residual and saturated water contents, respectively, α and *n* are the fitting parameters which control position and steepness of HEMC, respectively, A, B and C are quadratic fitting coefficients. $\theta_{s\text{-Observed}}$ is water content measured at *h* value of 2 hPa.

Table 4
Correlation coefficients between the studied land-uses.

	EC	OM	BD	Clay	Sand	CCE	D	MWD
EC	1							
OM	−0.312**	1						
BD	0.103	−0.428**	1					
clay	−0.291**	0.475**	−0.570**	1				
sand	0.317**	−0.587**	0.578**	−0.870**	1			
CCE	−0.112	0.203*	−0.364**	0.590**	−0.621**	1		
D	0.301**	−0.552**	0.565**	−0.829**	0.814**	−0.483**	1	
MWD	−0.036	0.082	−0.146	0.311**	−0.327**	0.369**	−0.274**	1
VDP_{FW}	0.329**	−0.369**	0.413**	−0.759**	0.793**	−0.630**	0.619**	−0.372**
VDP_{SW}	0.271**	−0.331**	0.378**	−0.714**	0.769**	−0.655**	0.571**	−0.361**
SI_{FW}	0.307**	−0.311**	0.339**	−0.574**	0.603**	−0.500**	0.428**	−0.326**
SIsw	0.057	−0.273**	0.245*	−0.386**	0.456**	−0.383**	0.257**	−0.343**
SR	0.189	−0.001	0.034	−0.185	0.097	−0.076	0.092	0.014
$S_{i\text{-}FW}$	0.235*	−0.3**	0.36**	−0.68**	0.696**	−0.574**	0.52**	−0.378**
S_iR	0.168	0.028	0	−0.126	0.14	−0.065	0.162	−0.086
α_{FW}	−0.018	0.104	−0.102	0.333**	−0.347**	0.201*	−0.322**	−0.064
n_{FW}	0.068	−0.075	0.049	−0.191	0.203*	−0.135	0.124	−0.096
α_{SW}	−0.174	0.054	−0.071	0.304**	−0.295**	0.204*	−0.254*	−0.066
n_{SW}	0.117	−0.055	0.102	−0.281**	0.291**	−0.227*	0.283**	0.026
VDPR	0.337**	−0.360**	0.347**	−0.447**	0.471**	−0.245*	0.439**	−0.161

	VDP_{FW}	VDP_{SW}	SI_{FW}	SI_{SW}	SR	$S_{i\text{-}FW}$	SiR	α_{FW}	n_{FW}	α_{SW}	n_{SW}	VDPR
VDP_{FW}	1											
VDP_{SW}	0.959**	1										
SI_{FW}	0.826**	0.759**	1									
SI_{SW}	0.603**	0.633**	0.731**	1								
SR	0.252*	0.108	0.378**	−0.147	1							
$S_{i\text{-}FW}$	0.898**	0.876**	0.799**	0.622**	0.147	1						
SiR	0.287**	0.256*	0.201*	−0.064	0.202*	0.201*	1					
α_{FW}	−0.405**	−0.398**	0.078	0.131	0.046	−0.26**	−0.227*	1				
n_{FW}	0.224*	0.302**	−0.010	−0.035	−0.127	0.269**	0.089	−0.209*	1			
α_{SW}	−0.375**	−0.412**	−0.003	0.370**	−0.301**	−0.271**	−0.357**	0.682**	−0.325**	1		
n_{SW}	0.271**	0.262**	0.005	−0.193	0.137	0.293**	0.111	−0.395**	0.363**	−0.481**	1	
VDPR	0.576**	0.401**	0.531**	0.358**	0.103	0.518**	0.259**	−0.255*	−0.107	0.029	0.090	1

*, ** significant at $P < 0.05$ and $P < 0.01$ probability levels, respectively. BD and OM are bulk density and organic matter, respectively. CCE and D are calcium carbonate equivalent and fractal dimension, respectively. MWD is mean weight diameter of aggregates. VDP_{FW} and VDP_{SW} are VDP values in the fast and slow wetting modes, respectively. SI_{FW} and SI_{SW} are structural index in fast and slow wetting modes, respectively. SR is stability ratio, $S_{i\text{-}FW}$ the slope of HEMC at the inflection point and S_iR physical quality index ratio. α and *n* are the fitting parameters which control position and steepness of HEMC, respectively. VDPR is the ratio of VDP_{FW} to VDP_{SW}.

to having higher organic matter and clay content (Fig. 3a, g). Under the fast wetting mode, these aggregates would breakdown and consequently, the value of $\theta_{s\text{-observed}}$ for the undisturbed rangeland approached the values reported for disturbed rangeland and artificial forest plantation land-use types (Table 3 and Fig. 2b). Mamedov et al. (2016) argues that HEMC is a function of various soil properties, amongst them is bulk density (BD). The near-saturated water content value of the protected forest (L3) in both fast and slow wetting modes was almost similar and lower compared to other land-use types (Fig. 2a, b). This could be attributed to the weak soil structure as well as frequent sand-sized soil particles in the protected forest (Table 1). The effective pore diameter at the interface menisci location of the fast and slow curves was calculated based on the report of Kelishadi et al. (2018). The effective pore diameter for the L3 location was 375 μm and for the other land use types was obtained by almost 250 μm. Since the values of HEMC indices for the L3 were also high, one can conclude that the effective diameter could be influenced by soil texture as well as sand particles. In Brazil, Silva et al. (2014) showed that HEMC is a function of land-use type and management. One can expect significant changes in the HEMC when soil structure is improved. The results showed that the water retention data were higher in slow wetting mode compared to fast wetting one (Fig. 2c and Table 3**(**. During the fast wetting mode, due to the effect of entrapped air in the pores, hydration of exchangeable cations and clay surfaces and heterogeneous swelling, the aggregates breakdown was higher than the slow wetting mode. In general, aggregate breakdown by fast wetting results in the formation of small pores, which consequently leads to decreased VDP (Hosseini et al., 2015; Mamedov et al., 2017; Gholoubi et al., 2019; Saffari et al., 2020). Many researchers have reported the negative impact of soil structural degradation on soil water retention (Sillers et al., 2001; Baumgartl and Kock, 2004; Dexter et al., 2008). Silva et al (2014), compared the HEMC in both fast and slow wetting modes and stated that at the low suctions, the slow wetting curve was located higher (higher water content) than the fast wetting one. However, as the suction increases, the position of the two curves reverses.

The area between the specific water capacity curve and the shrinkage line shows the amount of VDP (Fig. 2d). In this study, the highest VDP was observed in the protected forest, followed by the artificial forest plantation, undisturbed rangeland and disturbed rangeland, respectively. Hosseini et al. (2015) reported that VDP and water content for the fine-textured soils were higher than the coarse-textured ones. This probably was due to higher clay content, lower sand content, and enhanced aggregation. However, in our research, higher values of VDP in the protected forest could not be attributed to the presence of coarse and resistant aggregates since these land uses were characterized by low aggregation with fine aggregates. Instead, these higher values for VDP seem to be due to large quantities of sand in the studied soils (Table 1). According to Dexter et al. (2008) soil pores are divided into textural and structural pores. It can be concluded that in this research the value of VDP was more representative of the textural pores.

Fig. 2e shows higher VDP values in the slow wetting than the fast wetting for the disturbed rangeland. The reason is that the fast wetting leads to aggregate breakdown and as a result, the amount of aggregates and the VDP decline in the fast wetting mode than the slow wetting one. These results are consistent with the findings of Levy and Mamedov (2002) and Hosseini et al. (2015). Hosseini et al. (2015) stated that the

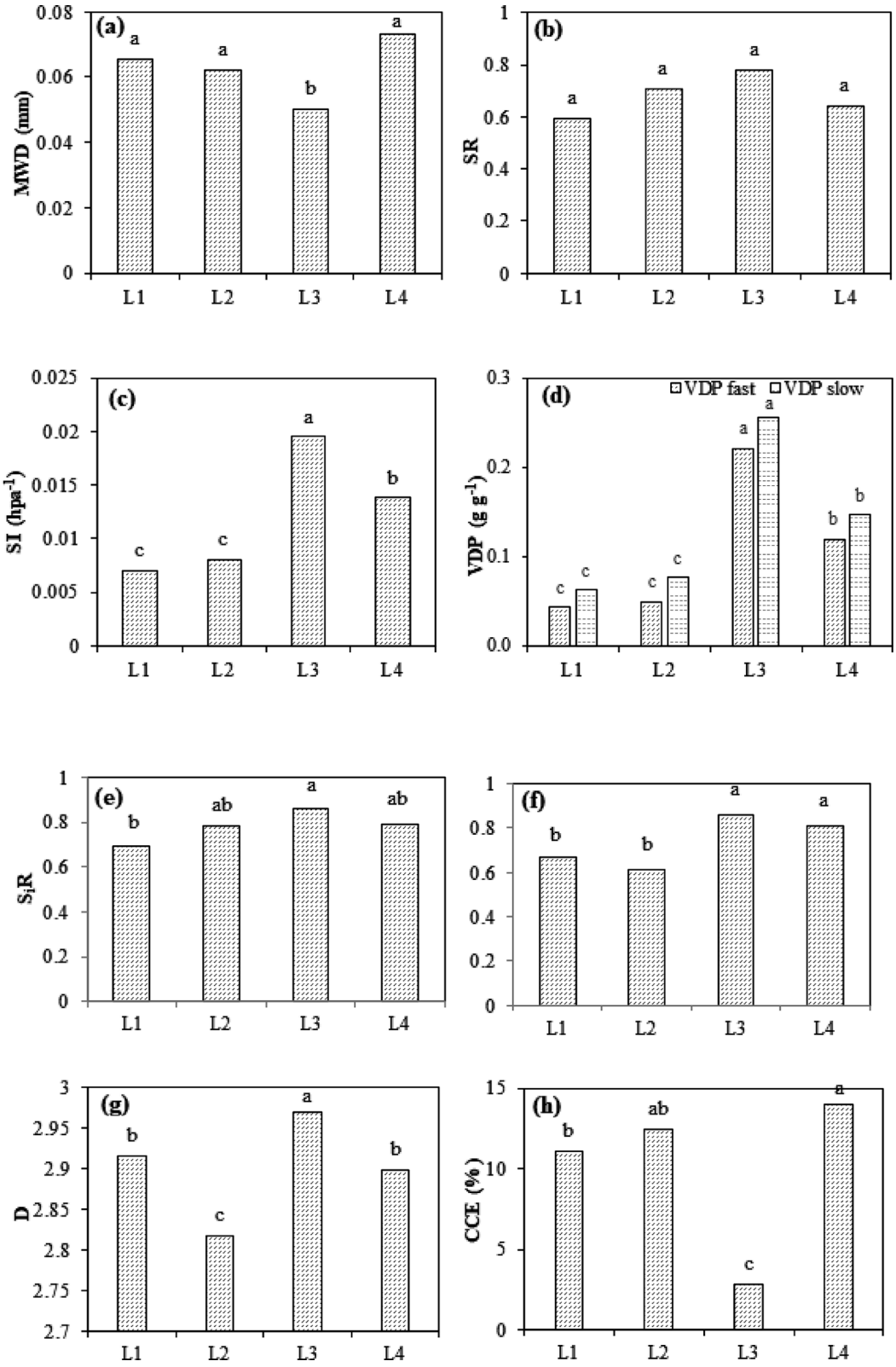

Fig. 3. Mean comparisons of (a) mean weight diameter of aggregates (MWD, mm), (b) stability ratio (SR), (c) structural index (SI, hPa^{-1}) of fast wetting aggregates, (d) volume of drainable pores (VDP, g g^{-1}) of fast wetting aggregates, (e) ratio of slopes at the inflection point (S_i) of HEMC of fast wetting to slow wetting aggregates (S_iR), (f) ratio of fast wetting to slow wetting VDP values (VDPR), (g) aggregate fractal dimension (D), (h) calcium carbonate equivalent (CCE, %), (i) geometric mean diameter (GMD, mm), (j) geometric standard deviation (GSD), in different land-uses. Different letters on the bars indicate significant differences (LSD, $P < 0.05$).

peak of the specific capacity curves represents the most frequent pore size. As the pore size becomes smaller due to fast wetting, the peak of the fast wetting curve occurs at a lower level than that of the slow wetting one. Furthermore, because the soil particle size and therefore the pore size were larger in the protected forest and artificial forest plantation compared to the other land-use types, these two land-use types showed a higher peak (Fig. 2d, e).

3.2. Land-use types and soil structural properties

Fig. 3 shows mean comparisons of some soil physical properties in different land use types. The MWD value (0.05 mm) was lower in L3 compared to other land-use types (Fig. 3a). The results of the correlation coefficient also indicate that the lower MWD value can be attributed to the lower percentage of clay and CCE as well as a higher percentage of sand in this treatment (Tables 1 and 4). In terms of SR index, there were no significant differences between the land-use types (Fig. 3b); however, significant differences were found for the SI index (Fig. 3c) with the highest value of the SI_{FW} index corresponded to L3 (0.0195 hPa^{-1}). The results of mean comparison for the VDP indicated a significant difference ($P < 0.05$) between different land-use types (Fig. 3d). The highest VDP obtained for the protected forest may be due to the high sand content (Table 1) and probably the uniform particle size distribution in this land use-type compared to other ones. Since the L4 site had less sand content (62.4 Kg $100Kg^{-1}$) compared to L3 (77.3 Kg $100Kg^{-1}$) (Table 1), its VDP was lower. As other soil properties in L1 and L4 land use types were somewhat similar, the differences observed for SI and VDP values were probably due to their particle size distribution; so that L4 represented higher sand content (62.4 Kg $100Kg^{-1}$) than L1 (59.1 Kg $100Kg^{-1}$). In addition, it is maybe due to higher levels of EC (Table 1) and CCE (Fig. 3h) in the artificial forest plantation (L4), which resulted in the higher rate of soil aggregation in this land-use type compared to the disturbed rangeland.

Moreover, VDP values for the protected forest and undisturbed rangeland sites decreased by 14% and 45% in the fast compared to the slow wetting mode, respectively (Fig. 2d). The decrease in the other two land-use types was <25%. This comparison indicates that the undisturbed rangeland represented higher number of as well as larger aggregates compared to the other land-use types. Fast wetting of these aggregates resulted in aggregates breakdown and consequently led to decreased soil porosity so that the decrease in VDP for undisturbed rangeland was higher than land-use types. These findings are consistent with the results of Gholoubi et al. (2019) who observed that aggregates breakdown into smaller aggregates by wetting (if these aggregates are not very stable), and pore size distribution shifts to a larger amount of micro-pores, thereby the VDP value is reduced. In this study, the high value of VDPR and S_iR were observed in the L3 and L4 land-use types. It could possibly be due to the unknown effect of some other factors such as the fine-structured soil, type of clay minerals, etc., which cannot be attributed to the higher sand content.

There were significant changes in the fractal dimension among the land-use types. The lowest and highest values of fractal dimension were observed for the L2 and L3 treatments, respectively (Fig. 3g). The lower fractal dimension indicates better soil structure and greater amounts of stable aggregates. Gulser (2006) reported that fractal dimension values increase with decreasing soil organic matter content. One of the important factors in the formation of soil aggregate is $CaCO_3$, which contributes in the binding of soil particles together, thereby forming the soil aggregate. The MWD value was lower In L3 land-use type compared to other ones mainly due to the low percentage of CCE (Fig. 3h, 3a).

3.3. Correlation of soil structural properties

The VDP_{FW} and VDP_{SW} were directly correlated with electrical conductivity (EC), structural index (SI), the ratio of VDP_{FW} to VDP_{SW} (VDPR), $S_{i\ -\ FW}$, and the ratio of $S_{i\ -\ FW}$ to $S_{i\ -\ SW}$ (S_iR). However, the VDP was inversely correlated with the organic matter content. No correlation was obtained between some of the HEMC indices and the amount of organic matter. Similarly, Levy and Mamedov (2002) examined aggregate stability in arid and semi-arid regions and observed a weak correlation between these indices and organic matter. Instead, in areas with high organic matter content, there is a strong correlation between these indices. Levy and Mamedov (2002) argued that the lack of a relationship between organic matter content and aggregate stability indices could be due to low organic matter content (<2%) in arid and semi-arid regions. Moreover, the results showed that there was no relationship between HEMC and clay content and CCE indices; instead, these indices directly correlated with soil electrical conductivity and sand content. As, indices such as VDP and SI could not differentiate between aggregate and sand particles, so these indices positively correlated with sand, while negatively with clay and organic matter. However, as mentioned earlier, another reason for the negative relationship between HEMC indices with clay and organic matter was their low content in the studied soils. The indices such as the aggregate fractal dimension are inversely correlated with organic matter, clay content, and CCE; instead, they have a direct relationship with bulk density.

In addition, in this study, the S_i (slope of HEMC at the inflection point) was measured as another index for evaluating soil structural stability. Hosseini et al. (2015) and Saffari et al. (2020) discussed that S_i could serve as a valuable index for evaluation and assessment of aggregate stability and other HEMC indices. There was a significant negative correlation between $S_{i\ -\ FW}$ and the clay and organic matter content while a positive correlation between $S_{i\ -\ FW}$ and the sand content indicated that this index, like other HEMC indices in this study, was more affected by the soil sand content and its properties (Table 4). High value of fractal dimension represents weak and fine aggregates so that aggregation could be improved with increasing factors such as organic matter, clay and calcium carbonate while the reverse trend is true for fractal dimension.

4. Conclusion

The results showed that soil structural behaviors particularly influenced on both near-saturated water content and soil water retention. Soils low in clay content, organic matter, and carbonate calcium equivalent as the aggregation and stability factors, showed lower levels of water retention and near-saturated water content. However, soil texture indicated a higher effect on high-energy moisture characteristic indices. Studies have demonstrated that soil intrinsic properties such as texture are of higher importance in determining some HEMC indices while structural properties such as aggregate stability are more suitable for other HEMC indices. Therefore, it can be concluded that only a few indices were sensitive to land management practices and land-use type. For the protected forests, these indices showed the highest values because of the sandy texture. Artificial forest plantation was characterized by lower sand content compared to the protected forest, thus the values of HEMC indices such as SI and VDP were lower in the artificial forest plantation. Since there was no significant difference between disturbed and undisturbed rangelands in terms of HEMC indices, it can be concluded that the disturbance had no significant influence on the aggregating processes for the studied region.

Declaration of Competing Interest

The authors declare that they have no known competing financial interests or personal relationships that could have appeared to influence the work reported in this paper.

Acknowledgment

The authors would like to appreciate and thank Ms. Neda Saffari of Isfahan University of Technology for helping modeling the HEMC data.

References

Amiri, I., Sodaiezade, H., Mosleh Arani, A., Taie Semiromi, J., Hakimzade, M.A., 2019. Autecology of Tecomella undulata (Roxb.) Seem in southern Iran. Journal of Forest and Poplar Research 26 (4):506–519 (In Persian with English abstract).

J.C. Avanzi L. Darrell N., Naves Silva, M.L., Curi, N., Hoffmann, A., da Silva, M. Aggregate stability in soils cultivated with eucalyptus Pesquisa Agropecuária Brasilia. 46 1 2011 89 96 10.1590/S0100-204X2011000100012.

Baiamonte, G., Crescimanno, G., Parrino, F., De Pasquale, C., 2019. Effect of biochar on the physical and structural properties of a desert sandy soil. Catena 175, 294–303. https://doi.org/10.1016/j.catena.2018.12.019.

Baranian Kabir, E., Bashari, H., Mosaddeghi, M.R., Bassiri, M., 2017. Soil aggregate stability and organic matter as affected by land use change in central Iran. Arch. Agron. Soil Sci. 63 (13), 1823–1837. https://doi.org/10.1080/03650340.2017.1308492.

Baumgartl, T., Kock, B., 2004. Modelling volume change and mechanical properties with hydraulic models. Soil Sci. Soc. Am. J. 68 (1), 57–65. https://doi.org/10.2136/sssaj2004.5700.

Blake, G.R., Hartge, K.H., 1986. Bulk density. In: Klute, A. (Ed.), Methods of Soil Analysis Part 1, Physical and Minerological Methods. Agronomy Monographs. 9, 2nd ed. ASA and SSSA, Madison, WI, 364–367.

Brtnicky, M., Elbl, J., Dvorackova, H., Kynicky, J., Hladky, J., 2017. Changes in soil aggregate stability induced by mineral nitrogen fertilizer application. Acta Uuniversitatis Agriculturae et Silviculturae Mendelianae Brunensis. 65 (5), 1477–1482. https://doi.org/10.11118/actaun201765051477.

C. Castro Filho A. Lourenco Guimaraes, M.de F., Fonseca I.C.B. Aggregate stability under different soil management systems in a red latosol in the state of Parana Brazil. Soil and Tillage Research 65 1 2002 45 51 10.1016/S0167-1987(01)00275-6.

Childs, E.C., 1940. The use of soil moisture characteristics in soil studies. Soil Sci. 50 (4), 239–252.

Collis-George, N., Figueroa, B.S., 1984. The use of high energy moisture characteristic to assess soil stability. Australian Journal Soil Research 22 (3), 349–356. https://doi.org/10.1071/SR9840349.

G. Crescimanno lovino, M., Provenzano, G. Influence of Salinity and Sodicity on Soil Structural and Hydraulic Characteristics Soil Science Society of America Journal. 59 6 1995 1701 1708 10.2136/sssaj1995.03615995005900060028x.

Y.T. Delelegn W. Purahong A. Blazevic B. Yitaferu T. Wubet goransson, H., Godbold, D.L. Changes in land use alter oil quality and aggregate stability in the highlands of northern Ethiopia Scientific Reports. 7 1 2017 13602 10.1038/s41598-017-14128-y.

Dexter, A.R., Czyz, E.A., Richard, G., Grunwald, A., 2008. A user-friendly water retention function that takes account of the textural and structural pore spaces in soil. Geoderma 143 (3–4), 243–253. https://doi.org/10.1016/j.geoderma.2007.11.010.

Ding, W., Huang, C., 2017. Effects of soil surface roughness on interrill erosion processes and sediment particle size distribution. Geomorphology 295, 801–810. https://doi.org/10.1016/j.geomorph.2017.08.033.

Dlapa, P., Chrenkova, K., Hrabovsky, A., Mataix-Solera, J., Kollar, J., Šimkovic, I., Jurani, B., 2011. The effect of land use on soil aggregate stability in the viticulture district of MODRA (SW Slovakia). Ecologia. 30 (4), 397–404. https://doi.org/10.4149/ekol-2011-04-397.

Gee, G.W., Bauder, J.W., 1986. Particle-size analyses In: Klute, A. (Ed.), Methods of Soil Analyses. Part 1: Physical and Mineralogical Methods, 2nd ed. Agronomy Monographs, vol. 9. ASA and SSSA, Madison, WI, pp. 383-411.

Gholoubi, A., Emami, H., Caldwell, T., 2019. Deforestation effects on soil aggregate stability quantified by the high-energy moisture characteristic method. Geoderma 355, 113919. https://doi.org/10.1016/j.geoderma.2019.113919.

Gulser, C., 2006. Effect of forage cropping treatments on soil structure and relationships with fractal dimensions. Geoderma 131 (1–2), 33–44. https://doi.org/10.1016/j.geoderma.2005.03.004.

Hillel, D., 1982. Introduction to soil physics, 1st ed. Academic Press, San Diego, CA.

Hosseini, F., Mosaddeghi, M.R., Hajabbasi, M.A., Sabzalian, M.R., 2015. Influence of tall fescue endophyte infection on structurel stability as quantified by high energy moisture characteristic in a range of soils. Geoderma 249–250, 87–99. https://doi.org/10.1016/j.geoderma.2015.03.013.

Kelishadi, H., Mosaddeghi, M.R., Ayoubi, S., Mamedov, A.I., 2018. Effect of temperature on structural stability as characterized by high energy moisture characteristic method. Catena 170, 290–304. https://doi.org/10.1016/j.catena.2018.06.015.

Le Bissonnais, Y., 1996. Aggregate stability and assessment of soil crustability and erodibility :I. Theory and methodology. Eur. J. Soil Sci. 47 (4), 425–437. https://doi.org/10.1111/j.1365-2389.1996.tb01843.x.

Levy, G.J., Mamedov, A.I., 2002. High energy moisture characteristic aggregate stability as a predictor for seal formation. Soil Sci. Soc. Am. J. 66 (5), 1603–1609. https://doi.org/10.2136/sssaj2002.1603.

Levy, G.J., Miller, W.P., 1997. Aggregate stabilities of some southeastern U.S. soils. Soil Sci. Soc. Am. J. 61, 1176–1182.

Mamedov, A.I., Huang, C., Aliev, F.A., Levy, G.J., 2017. Aggregate stability and water retention near saturation characteristics as affected by soil texture aggregate size and polyacrylamide application. Land Degrad. Dev. 28 (2), 543–552. https://doi.org/10.1002/ldr.2509.

Mamedov, A.I., 2014. Soil water retention and structure stability as affected by water quality. Eurasian Journal of Soil Science 3 (2), 89–94. https://doi.org/10.18393/ejss.24378.

Mamedov, A.I., Ekberli, I., Gulser, C., Gumus, I., Cetin, U., Levy, G.J., 2016. Relationship between soil water retention model parameters and structure stability. Eurasian Journal of Soil Science 5 (4), 314–321. https://doi.org/10.18393/ejss.2016.4.314-321.

, 1982McLean, E.O., 1982. Soil pH and lime requirement. In: Page, A.L. Miller, R.H. Keeney, D.R (Eds). Methods of Soil Analysis, Part 2. Chemical and microbiological Properties, Agronomy monograph, 2nd Ed Agronomy. 9: 199-224.

Nelson, D.W., Sommers, L.E., 1996. Total carbon, organic carbon and organic matter. In: Methods of soil Analysis, part 2., A.L. Page et al., Ed ed Agronomy, Page et al., Ed Agronomy 9:961-1010. American Society of Agronomy, Inc Madison, WI.

Pierson, F.B., Mulla, D.J., 1989. An improved method for measuring aggregate stability of a weakly aggregated loessial soil. Soil Sci. Soc. Am. J. 53 (6), 1825–1832. https://doi.org/10.2136/sssaj1989.03615995005300060057x.

Rhoades, J.D., 1996. Salinity: electrical conductivity and total dissolved solids. Methods of soil analysis, Part 3: Chemical Methods, Soil Science Society of America Madison, 417-435.

, 2011Roodab Paydar consulting engineers., 2011. Detailed studies of forest resources management plan in Tal Siah area, ministry of Agriculture. (In Persian).

Co, Sabznegar Afaq, 1999. Farrash rangeland plan, ministry of Agriculture. (In Persian).

Saffari, N., Hajabbasi, M.A., Shirani, H., Mosaddeghi, M.R., Mamedov, A.I., 2020. Biochar type and pyrolysis temperature effects on soil quality indicators and structural stability. J. Environ. Manage. 261, 110190.

, 2008Saman Sabz Ariyan consulting engineers., 2008. Marghzar rangeland plan, ministry of Agriculture. (In Persian).

Saygın, S.D., Cornelis, W.M., Erpul, G., Gabriels, D., 2012. Comparison of different aggregate stability approaches for loamy sand soils. Appl. Soil Ecol. 54, 1–6. https://doi.org/10.1016/j.apsoil.2011.11.012.

Sillers, W.S., Fredlund, D.G., Zakerzadeh, N., 2001. Mathematical attributes of some soil-water characteristic curve models. Geotech. Geol. Eng. 19, 243–283. https://doi.org/10.1023/A:1013109728218.

Silva, E.A., Oliveira, G.C., Silva, B.M., Carducci, C.E., Avanzi, J.C., Serafim, M.E., 2014. Aggregate stability by the high energy moisture characteristic method in an Oxisol under the differentiated management. Revista Brasileira de Ciência do Solo 38 (5), 1633–1642.

Sims, J.T., 1996. Lime requirement. In: Sparks, D.L., Page, A.L., Helmke, P.A., Loeppert, P.N., Soltanpour, P.N., Tabatabaei, M.A., Johnson, C.T., Sumner, M.E. (Eds.), Methods of Soil Analysis. Part 3. Cemical Methods, Second ed., Soil Science Society of America Journal. Book Series Number 5. ASA and SSSA, Madison, WI, 491-515.

Tang, F.K., Cui, M., Lu, Q., Liu, Y.G., Guo, H.Y., Zho, J.X., 2016. Effects of vegetation restoration on the aggregate stability and distribution of aggregate-associated organic carbon in a typical karst gorge region. Solid Earth 7, 141–151.

van Bavel, C.H.M., 1950. Mean weight diameter of soil aggregates as a statistical index of aggregation. Soil Science of America Journal 14, 20–23. https://doi.org/10.2136/sssaj1950.03615995001400OhbC0005x.

Yang, P.L., Luo, Y.P., Shi, Y.C., 1993. Fractal characteristics of soil by weight distribution of particle size. Chin. Sci. Bull. 38 (20), 1896–1899.

Zhang, K.L., Shu, A.P., Xu, X.L., Yang, Q.K., Yu, B., 2008. Soil erodibility and its estimation for agricultural soils in China. J. Arid Environ. 72 (6), 1002–1011. https://doi.org/10.1016/j.jaridenv.2007.11.018.

Zheng, Z.C., He, S.Q., Li, T.X., 2011a. Fractal dimensions of soil structure and soil anti-erodibility under different land use patterns. Afr. J. Agric. Res. 6 (24), 5496–5504. https://doi.org/10.5897/AJAR11.345. DOI: 10.5897/AJAR11.345.

Zheng, Z.C., He, S.Q., Li, T.X., Wang, Y.D., 2011b. Effect of land use patterns on stability and distributions of organic carbon in the hilly region of Western Sichuan. China. African Journal of Biotechnology 10 (61), 13107–13114. https://doi.org/10.5897/AJB10.237.